The effect of permafrost on time-split soil erosion using radionuclides (^{13}Cs, ^{239,240}Pu, meteoric ^{10}Be) and stable isotopes (^{13}C) in the eastern Swiss Alps

Zollinger, Barbara ; Alewell, Christine ; Kneisel, Christof ; Meusburger, Katrin ; Brandová, Dagmar ; Kubik, Peter ; Schaller, Mirjam ; Ketterer, Michael ; Egli, Markus

Abstract: Purpose: Global warming is expected to change the thermal and hydrological soil regime in permafrost ecosystems which might impact soil erosion processes. Erosion assessment using radionuclides can provide information on past and ongoing, i.e. time-split, processes. The focus of this work was to find out if permafrost soils in the Swiss Alps differ in their medium- and long-term erosion rates from non-permafrost soils and if rates have accelerated during the last few decades. Materials and methods: Using cosmogenic (meteoric ^{10}Be) and anthropogenic radionuclides (^{137}Cs, ^{239,240}Pu), a time-split approach was achieved by determining erosion activities on the long (millennia; ^{10}Be) and medium term (decades; ^{137}Cs, ^{239,240}Pu). Additionally, the stable isotope ^{13}C signature in soil organic matter was used as a qualitative indicator for soil disturbance patterns. We compared soil erosion processes in permafrost soils and nearby unfrozen soils in the alpine (sites at 2,700 m asl, alpine tundra) and the subalpine (sites 1,800 m asl, natural forest) range of the Swiss Alps (Upper Engadine). ^{137}Cs, ^{239,240}Pu and ^{13}C measurements were performed at the alpine sites only. Results and discussion: Depending on the calculation procedure (profile distribution model or inventory method), the ^{137}Cs measurements revealed soil accumulation rates of 1–3 t/km²/year in permafrost soils and 34–52 t/km²/year in non-permafrost soils. However, due to snow cover and subsequent melt-water runoff during ^{137}Cs deposition after the Chernobyl accident, caesium does not seem to be an appropriate soil erosion tracer on the investigated alpine sites. With ^{239,240}Pu, more reliable results were achieved. ^{239,240}Pu measurements provided erosion rates of 31–186 t/km²/year in permafrost soils and accumulation rates of 87–218 t/km²/year in non-permafrost soils. Erosion and accumulation were relatively low and related to the vegetation community. The long-term (^{10}Be) soil redistribution rates (erosion rates up to 49 t/km²/year and accumulation rates up to 4 t/km²/year) were low with no significant differences between permafrost and non-permafrost sites. The ^{13}C signature indicated soil disturbances in permafrost and non-permafrost soils compared to the reference site. Conclusions: Our results highlight that soil redistribution rates have increased during the last few decades. However, whether the higher medium-term erosion rates obtained for the last decades are the result of the ongoing climate warming and related accelerated soil erosion or if other factors (e.g. measurement uncertainties) have been responsible for such an increase could not fully be clarified.

DOI: https://doi.org/10.1007/s11368-014-0881-9

Zollinger, Barbara; Alewell, Christine; Kneisel, Christof; Meusburger, Katrin; Brandová, Dagmar; Kubik, Peter; Schaller, Mirjam; Ketterer, Michael; Egli, Markus (2015). The effect of permafrost on time-split soil erosion using radionuclides (^{13}Cs, ^{23} ^{2} Pu, meteoric ^{1}Be) and stable isotopes (^{13}C) in the eastern Swiss Alps. Journal of Soils and Sediments, 15(6):1400-1419.
DOI: https://doi.org/10.1007/s11368-014-0881-9

J Soils Sediments (2015) 15:1400–1419
DOI 10.1007/s11368-014-0881-9

SOIL FORMATION AND WEATHERING IN TIME AND SPACE

The effect of permafrost on time-split soil erosion using radionuclides (^{137}Cs, $^{239+240}$Pu, meteoric ^{10}Be) and stable isotopes (δ^{13}C) in the eastern Swiss Alps

Barbara Zollinger · Christine Alewell · Christof Kneisel · Katrin Meusburger · Dagmar Brandová · Peter Kubik · Mirjam Schaller · Michael Ketterer · Markus Egli

Received: 10 December 2013 / Accepted: 26 February 2014 / Published online: 26 March 2014

Abstract
Purpose Global warming is expected to change the thermal and hydrological soil regime in permafrost ecosystems which might impact soil erosion processes. Erosion assessment using radionuclides can provide information on past and ongoing, i.e. time-split, processes. The focus of this work was to find out if permafrost soils in the Swiss Alps differ in their medium- and long-term erosion rates from non-permafrost soils and if rates have accelerated during the last few decades.
Materials and methods Using cosmogenic (meteoric ^{10}Be) and anthropogenic radionuclides (^{137}Cs, $^{239+240}$Pu), a time-split approach was achieved by determining erosion activities on the long (millennia; ^{10}Be) and medium term (decades; ^{137}Cs, $^{239+240}$Pu). Additionally, the stable isotope δ^{13}C signature in soil organic matter was used as a qualitative indicator for soil disturbance patterns. We compared soil erosion processes in permafrost soils and nearby unfrozen soils in the alpine (sites at 2,700 m asl, alpine tundra) and the subalpine (sites 1,800 m asl, natural forest) range of the Swiss Alps (Upper Engadine). ^{137}Cs, $^{239+240}$Pu and δ^{13}C measurements were performed at the alpine sites only.
Results and discussion Depending on the calculation procedure (profile distribution model or inventory method), the ^{137}Cs measurements revealed soil accumulation rates of 1–3 t/km^2/year in permafrost soils and 34–52 t/km^2/year in non-permafrost soils. However, due to snow cover and subsequent melt-water runoff during ^{137}Cs deposition after the Chernobyl accident, caesium does not seem to be an appropriate soil erosion tracer on the investigated alpine sites. With $^{239+240}$Pu, more reliable results were achieved. $^{239+240}$Pu measurements provided erosion rates of 31–186 t/km^2/year in permafrost soils and accumulation rates of 87–218 t/km^2/year in non-permafrost soils. Erosion and accumulation were relatively low and related to the vegetation community. The long-term (^{10}Be) soil redistribution rates (erosion rates up to 49 t/km^2/year and accumulation rates up to 4 t/km^2/year) were low with no significant differences between permafrost and non-permafrost sites. The δ^{13}C signature indicated soil disturbances in permafrost and non-permafrost soils compared to the reference site.
Conclusions Our results highlight that soil redistribution rates have increased during the last few decades. However, whether the higher medium-term erosion rates obtained for the last decades are the result of the ongoing climate warming and related accelerated soil erosion or if other factors (e.g. measurement uncertainties) have been responsible for such an increase could not fully be clarified.

Responsible editor: Fabio Scarciglia

B. Zollinger (✉) · D. Brandová · M. Egli
Department of Geography, University of Zurich, Winterthurerstrasse 190, 8057 Zurich, Switzerland
e-mail: barbara.zollinger@geo.uzh.ch

C. Alewell · K. Meusburger
Environmental Geosciences, Department of Environmental Sciences, University of Basel, Bernoullistrasse 30, 4056 Basel, Switzerland

C. Kneisel
Institute of Geography and Geology, University of Würzburg, Am Hubland, 97074 Würzburg, Germany

P. Kubik
Laboratory of Ion Beam Physics, ETH Zürich, Schafmattstrasse 20, 8093 Zurich, Switzerland

M. Schaller
Geodynamics, University of Tübingen, Wilhelmstrasse 56, 72076 Tübingen, Germany

M. Ketterer
Chemistry Department, Metropolitan State University of Denver, Campus Box 52, Denver, CO 80217-3362, USA

Keywords Alpine soils · Anthropogenic/cosmogenic radionuclides · Climate · Isotopes

1 Introduction

Alpine landscapes and their features such as glaciers, permafrost and cold soils are climate sensitive and are expected to experience considerable changes in the future. Statistical relations and energy balance considerations indicate that one third to one half of the current mountain glacier mass could disappear over the next 100 years with a warming of 4 °C (according to IPCC scenarios; Jóhannesson et al. 1989; Hoelzle et al. 2003; Haeberli et al. 2004). With an upward shift of the equilibrium line by some 200 to 300 m, yearly thickness losses of 1 to 2 m are expected from temperate glaciers, and many low-latitude mountain chains such as the European Alps would lose major parts of their glacier cover within decades. As a further consequence, permafrost thawing might affect the potential starting zones of natural hazards (rockfall, mudflows) and the dynamics of processes (soil, vegetation; Haeberli et al. 2007). Consequently, a decline in permafrost due to climate warming might have crucial consequences on slope stability and soil erosion processes in Alpine areas (Kääb et al. 2007; Scheurer et al. 2009). However, empirical measurements (in soils) are either missing or are controversially discussed. Tape et al. (2011), for example, observed a decline of erosion in the Alaskan Arctic since 1980.

Permafrost is a common phenomenon in cold alpine environments that are characterised by a rugged topography and extreme climatic conditions (Haeberli et al. 2010). Discontinuous permafrost distribution in the Alps can be assumed to potentially occur at north-facing sites above an altitude of 2,400 m asl and on south-facing sites above 3,000 m asl, respectively (Nötzli and Gruber 2005). Below the timberline, at very shaded sites, sporadic permafrost can additionally exist (Kneisel et al. 2000).

Topography, vegetation cover, soil texture, land-use management and rainfall patterns are the main drivers for soil erosion (Wischmeier and Smith 1978). Furthermore, snow processes (e.g. avalanches, snow gliding) and melt-water runoff processes are important erosive agents in mountain environments (Konz et al. 2010; Freppaz et al. 2010; Lana-Renault et al. 2011; Ceaglio et al. 2012). Few studies exist on soil erosion measurement and quantification under different land-use management at different mountain ranges (Alewell et al. 2008; Konz et al. 2010). Soil erosion studies in uncultivated alpine (permafrost) environments are scarce due to the difficult accessibility, high small-scale heterogeneity and complexity of processes. Furthermore, time-split approaches that differentiate between long-term (millennia) and medium-term (decades) processes are missing.

Fallout radionuclides (e.g. ^{137}Cs, ^{7}Be, ^{210}Pb$_{ex}$) have been successfully used worldwide for soil redistribution measurements since the 1970s (Zapata 2002; Ritchie and Ritchie 2007; Mabit et al. 2013). Konz et al. (2009) first tested the usability of the artificial radionuclide ^{137}Cs for estimating medium-term soil erosion on Swiss alpine grassland soils.

^{137}Cs was released during nuclear weapon testing from the 1950s to the 1960s and more regionally after the Chernobyl nuclear accident in 1986. Since ^{137}Cs (^{137}Cs $t_{1/2}$=30.2 years) was heterogeneously deposited over a relatively short time period after the Chernobyl accident (Alewell et al. 2013), the application of the more homogenously distributed $^{239+240}$Pu (^{239}Pu $t_{1/2}$=24,110 years; ^{240}Pu $t_{1/2}$=6,563 years) also attracts attention. $^{239+240}$Pu was globally dispersed during thermonuclear weapon testing mainly between 1952 and 1964 (Ketterer and Szechenyi 2008). The artificial radionuclides ^{137}Cs and $^{239+240}$Pu are deposited with rainfall and are strongly adsorbed on the soil surface. Depending on the timing of the main fallout, ^{137}Cs and $^{239+240}$Pu have the potential to estimate medium-term (25–60 years) soil redistribution. The method is based on estimations of net soil erosion/deposition rates from the differences of ^{137}Cs and $^{239+240}$Pu inventories measured at a study site to those established at an adjacent reference site, which is not affected by soil redistribution processes. In recent years, only few studies have investigated the potential of $^{239+240}$Pu as soil erosion tracer (Schimmack et al. 2001; Everett et al. 2008; Ketterer and Szechenyi 2008; Tims et al. 2010; Hoo et al. 2011; Alewell et al. 2013).

Long-term soil erosion rates (over millennia) can be assessed, among other methods, by using meteoric ^{10}Be (^{10}Be $t_{1/2}$=1.36 Myears). Meteoric ^{10}Be is produced in the atmosphere by cosmogenic ray spallation of nitrogen and oxygen and scavenged out of the atmosphere by precipitation. For more than 20 years, meteoric ^{10}Be is used to trace and quantify processes such as soil production and erosion rates (e.g. McKean et al. 1993) or to estimate soil residence times (Pavich et al. 1986). Soil erosion can be estimated by comparing the effective inventory of meteoric ^{10}Be measured in the soil with the theoretically calculated abundance for the expected age (Maejima et al. 2005; Tsai et al. 2008; Egli et al. 2010). Alpine soils have been developed over the last 20 kyears and are still not in a steady-state condition. Hence, Egli et al. (2010) could show that the application of a non-steady-state approach to estimate soil erosion rates achieves more reliable results than calculation procedures based on steady-state assumptions (e.g. Lal 2001). The determination of long-term soil erosion rates using meteoric ^{10}Be in alpine landscapes together with a non-steady-state approach has been, until now, very rarely been done.

An additional fast and cost-effective method to qualitatively assess soil disturbances on alpine soils is based on the δ^{13}C signature along soil profiles that enables to qualitatively describe soil disturbances more on a medium- to long-term time

scale (Schaub and Alewell 2009; Alewell et al. 2011; Meusburger et al. 2013). For undisturbed oxic soils, the $\delta^{13}C$ signature tends to become less negative (relative increase in the heavier ^{13}C) with soil depth (Alewell et al. 2011). We expect that the enrichment of $\delta^{13}C$ with soil depth, due to fractionation during decomposition, goes in parallel with a decrease in carbon content. Soil erosion processes have been shown to weaken this correlation (Schaub and Alewell 2009; Meusburger et al. 2013).

The aim of this investigation was to study medium- and long-term soil erosion on alpine soils and to derive time-split rates. By comparing permafrost soils with nearby non-permafrost soils at the alpine and subalpine range in the south-eastern Swiss Alps, the following questions have been addressed:

1. Do permafrost soils in the Alps differ in their medium- and long-term erosion rates from non-permafrost soils?
2. Are the estimated soil erosion rates based on the anthropogenic radionuclides ^{137}Cs and $^{239+240}Pu$ comparable?
3. Can the soil redistribution patterns also be qualitatively determined using the isotope $\delta^{13}C$ signature in soil profiles?

2 Materials and methods

2.1 Study area

The three study sites Val Bever (46° 32′ 34″ N, 9° 48′ 1″ E), Spinas (46° 33′ 18″ N, 9° 51′ 28″ E) and Albula (46° 34′ 35″ N, 9° 53′ 16″ E) are located in the Upper Engadine (Switzerland) (Fig. 1). The Lateglacial and Holocene history of the Upper Engadine area is well documented (e.g. Suter 1981; Böhlert et al. 2011). The soils are classified as skeleton-rich Cambisols, Cryosols or Podzols (Table 1; IUSS Working Group WRB 2007). The glacial till deposited in these areas consists of granite/gneiss (Julier Granite). According to soil taxonomy (Soil Survey Staff 2010), the soil moisture regime is udic (humid conditions, <90 days per year having a dry soil) at all sites and the soil temperature regime is cryic (mean annual temperature <8 °C). Maximum precipitation occurs during the summer and autumn months. Two alpine and one subalpine site were selected (Fig. 1, Table 1).

1. Alpine areas (Val Bever and Albula):

These sites are situated at approximately 2,700 m asl. For both alpine sites, a permafrost distribution map was available (Böckli et al. 2012). Furthermore, the occurrence of permafrost was inferred using two-dimensional geoelectrical soundings and near surface temperature measurements (iButton® DS1922L) at the Val Bever sites (Table 2). Geoelectrical measurements indicated the occurrence of an ice-poor permafrost in the bedrock. The depth of the permafrost table and thickness of the active layer could not in each case be derived from these measurements. In general, permafrost was at <2 m depth at the Bever site. Permafrost soils are favoured at north-facing slopes, whereas non-permafrost sites are found at south-facing sites. Cryoturbation features, which are common in permafrost soils, could be found at the Val Bever permafrost sites (Fig. 1, Table 1). At the Val Bever sites, the permafrost soils showed a scarce vegetation cover dominated by the vegetation community *Caricetum curvulae* (with the exception of one non-permafrost site where the *C. curvulae* community was also found). The vegetation community *Geo Montani-Nardetum* dominated the non-permafrost sites and developed a relatively dense vegetation cover. At the Albula site, the vegetation community *C. curvulae* dominated the permafrost sites, but developed a relatively dense vegetation cover as compared to the Val Bever site. At the non-permafrost soils, the vegetation consisted in the vegetation communities *C. curvulae* and *Empetro-vaccinetum* (Ericaceaeous dwarf shrubs).

2. Subalpine area (Spinas):

This site is located below the timberline at 1,800 m asl (at present, the timberline is between 2,200 and 2,300 m asl) and represents one of the special places where isolated permafrost lenses could be confirmed by several geophysical techniques and borehole drilling also at lower altitudes (Kneisel et al. 2000; Kneisel 2010). The active layer thickness usually ranged from 2 to 3 m. It is the only site situated in a forest. Mean annual air temperature is 1 °C and the mean annual precipitation is 1,050 mm (Schwarb et al. 2000). Permafrost lenses and nearby sites without permafrost could both be found at north-facing scree slopes due to differences in the microrelief and therefore site-specific climatology. There was no difference in the vegetation cover between the permafrost and non-permafrost soils, except the dense moss cover at some of the permafrost sites. The forest community is a *Larici-Pinetum cembrae*, with blueberry (*Vaccinium myrtillus*) and cranberry (*Vaccinium vitis-idaea*) in the under storey.

2.2 Experimental setup and soil sampling

In September 2011, at each site (i.e. Val Bever, Spinas, Albula), six soil profiles (half of them having permafrost and half of them without permafrost) were dug down to the C or BC horizon. The profiles were chosen in the middle of the slope, with the exception of two profiles: at the Albula site, one non-permafrost profile was situated in the upper part of the slope (‘A1o’; Table 1); at the Val Bever site, one permafrost profile was situated on a flat position (‘B1m’; Table 1).

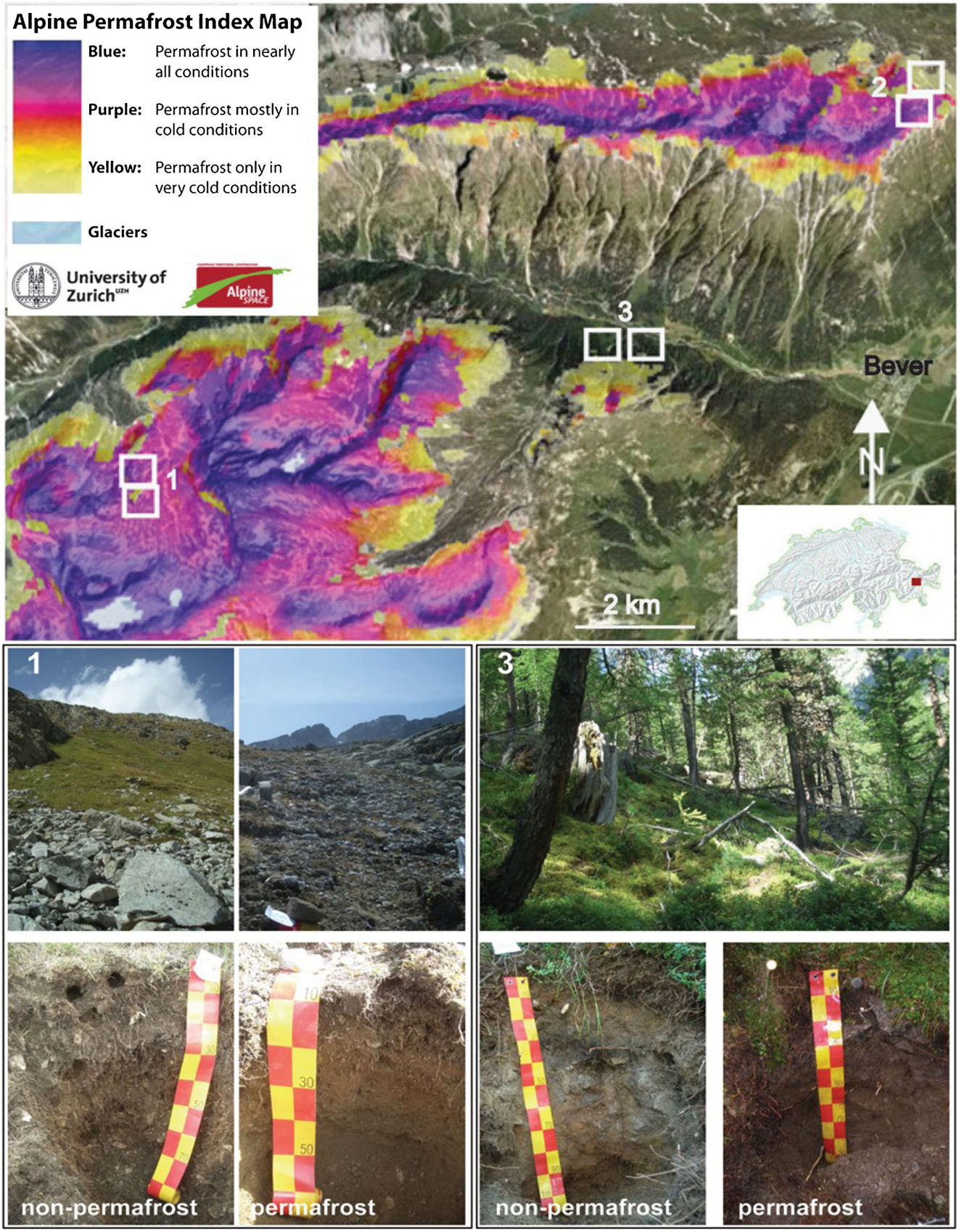
Alpine Permafrost Index Map
Blue: Permafrost in nearly all conditions
Purple: Permafrost mostly in cold conditions
Yellow: Permafrost only in very cold conditions
Glaciers
University of Zurich
Alpine Space
1
2
3
Bever
N
2 km
non-permafrost
permafrost
non-permafrost
permafrost

◀ **Fig. 1** Locations of the sampling sites in the Upper Engadine, close to the village Bever (46° 33′ 8″ N, 9° 53′ 20″ E), Switzerland. *1* 'Val Bever' (alpine sites with and without permafrost, vegetation: alpine tundra), *2* 'Albula' (alpine sites with and without permafrost, vegetation: alpine tundra), *3* 'Spinas' (subalpine sites with and without permafrost, vegetation: natural forest). The spatial permafrost model is run with a high-resolution (<1 km) global elevation data and air temperatures based on the NCAR-NCEP reanalysis and CRU TS 2.0 (Gruber 2012)

Approximately 2 to 4 kg of soil (cf. Hitz et al. 2002) was collected per horizon. Soil bulk density was determined using a soil core sampler (Eijkelkamp, volume 100.14 cm^3).

The profile samples were used for further meteoric ^{10}Be analysis. The ^{10}Be concentration was measured in the fine earth of each soil horizon (composite samples of three profiles for each situation: permafrost and non-permafrost soils).

For the assessment of soil erosion and soil disturbance using ^{137}Cs, $^{239+240}Pu$ and $\delta^{13}C$, an additional profile (termed reference profile) was sampled where erosion and accumulation processes can be neglected due to its flat topography. Soil samples for ^{137}Cs and $^{239+240}Pu$ analysis were collected using an 8-cm diameter soil core sampler. Soil cores were taken from 0 to 15 cm soil depth at each site around each profile (reference site (n=6), permafrost site (n=8) and non-permafrost site (n=8)). The soil cores were also used to determine the soil bulk densities. To establish the $\delta^{13}C$ depth profiles, samples were taken in 5 cm intervals from 0 to 50 cm soil depth in each soil profile (same profiles as for the ^{10}Be analysis).

The long-term erosion rate ^{10}Be measurements were performed for all three sites (the alpine and subalpine range 'Val Bever', 'Albula', 'Spinas'). ^{137}Cs and $^{239+240}Pu$ measurements were performed for the alpine sites 'Val Bever' only, while stable isotope ($\delta^{13}C$) measurements were performed for the alpine range 'Val Bever' and 'Albula'.

2.3 Soil chemistry and physics

Total C and N contents of the soil were measured with a C/H/N analyser (Elementar Vario EL). Soil pH (in 0.01 M $CaCl_2$) was determined on air-dried fine earth samples using a soil/solution ratio of 1:2.5. As the soils did not contain inorganic carbon (parent material: Julier granite), the total C contents equal the organic carbon content.

After a pre-treatment of the samples with H_2O_2 (3 %), particle size distribution of the soils was measured using a combined method consisting of wet-sieving the coarser particles (2,000–32 μm) and the measurement of the finer particles (<32 μm) by means of an X-ray sedimentometer (SediGraph 5100).

2.4 Analysis of ^{137}Cs activities

The activities of ^{137}Cs in the soil samples were determined by gamma spectrometry using a Li-drifted Germanium detector (20 % relative efficiency) at the Department for Physics and Astronomy, University of Basel. The counting time for each sample reached 28,800 to 43,200 s to obtain an acceptable level of measurement error. Calibration of equipment, analysis and quality control of the measurements were performed following IAEA standard procedure (Shakhashiro and Mabit 2009).

2.5 Analysis of $^{239+240}Pu$ activities

The measurement of Plutonium isotopes ($^{239+240}Pu$) was performed using a Thermo X Series II quadrupole ICP-MS instrument located at the Northern Arizona University. The ICP-MS instrument was equipped with a high-efficiency desolvating sample introduction system (APEX HF, ESI Scientific, Omaha, NE, USA). A detection limit of 0.1 Bq/kg $^{239+240}Pu$ was obtained for the samples of nominal 1 g of dry-ashed material; for $^{239+240}Pu$ activities >1 Bq/kg, the measurement error was 1 to 3 %. Prior to mass spectrometry analysis, the samples were dry-ashed and spiked with ~0.005 Bq of a ^{242}Pu yield tracer (obtained as a licensed solution from NIST). Pu was leached with 16 mol/l nitric acid overnight at 80 °C and was subsequently separated from the leach solution using a Pu-selective TEVA resin (Ketterer et al. 2011). The masses of ^{239}Pu and ^{240}Pu present in the sample, determined by isotope dilution calculations, were converted into the summed activity $^{239+240}Pu$ as has long been used in alpha spectrometric determinations of Pu activity. The $^{240}Pu/^{239}Pu$ atom ratios were determined in the same analytical run. Data quality was evaluated through the analysis of preparation blanks (soils or rocks devoid of Pu), duplicates and control samples having known $^{239+240}Pu$ activities.

2.6 Analysis of meteoric ^{10}Be activities

^{10}Be was extracted from the soil samples using a modified method from Horiuchi et al. (1999) (see Egli et al. 2010). The $^{10}Be/^{9}Be$ ratios were measured at the ETH Zurich Tandem Accelerator Mass Spectrometry (AMS) facility (Kubik and Christl 2009) using ETH AMS standards S2007N ($^{10}Be/Be = 28.1\times10^{-12}$ nominal) and ICN 01-5-1 ($^{10}Be/^{9}Be = 2.709\times10^{-11}$ nominal) (Nishiizumi et al. 2007) both associated with a ^{10}Be half-life of 1.387±0.012 Myears.

2.7 Analysis of $\delta^{13}C$ signature

Samples were dried in the oven at 40 °C and sieved (<2 mm) prior to analysis. Stable carbon isotope and total carbon analyses were accomplished using a continuous flow isotope ratio mass spectrometer (DELTAplus XP, Thermo Finnigan, Bremen, Germany) coupled with

Table 1 Characteristics of the study sites

Site	Coordinates[a] (N/E)	Elevation (m asl)	Aspect (°N)	Slope (%)	Parent material	Vegetation	Soil orders (WRB[b])
Non-permafrost sites: alpine							
Val Bever							
B1o	46° 32′ 27″/9° 47′ 52″	2,695	120	70	Granite/gneiss (Julier Granite)	Alpine tundra (*Geo Montani-Nardetum*)	Entic Podzol
B2o	46° 32′ 32″/9° 47′ 53″	2,680	120	78	Granite/gneiss (Julier Granite)	Alpine tundra (*Geo Montani-Nardetum*)	Haplic Regosol (humic)
B3o	46° 32′ 30″/9° 47′ 54″	2,677	120	36	Granite/gneiss (Julier Granite)	Alpine tundra (*Caricetum curvulae*)	Entic Podzol
Albula							
A1o	46° 34′ 33″/9° 53′ 14″	2,615	150	70	Granite/gneiss (Julier Granite)	Alpine tundra (*Caricetum curvulae*)	Entic Podzol
A2o	46° 34′ 35″/9° 53′ 17″	2,577	160	40	Granite/gneiss (Julier Granite)	Alpine tundra (*Caricetum curvulae*)	Entic Podzol
A3o	46° 34′ 34″/9° 53′ 17″	2,569	160	42	Granite/gneiss (Julier Granite)	Alpine tundra (*Empeto-vaccinetum*)	Entic Podzol
Non-permafrost sites: subalpine							
Spinas							
S1o	46° 33′ 18″/9° 51′ 29″	1,820	26	57	Granite-rich slope deposits	Natural forest (*Larici-Pinetum cembrae)*	Albic Podzol
S2o	46° 33′ 18″/9° 51′ 29″	1,820	26	57	Granite-rich slope deposits	Natural forest (*Larici-Pinetum cembrae*)	Albic Podzol
S3o	46° 33′ 18″/9° 51′ 34″	1,796	40	46	Granite-rich slope deposits	Natural forest (*Larici-Pinetum cembrae*)	Haplic Podzol
Permafrost sites: alpine							
Val Bever							
B1m	46° 32′ 36″/9° 47′ 57″	2,674	30	0	Granite/gneiss (Julier Granite)	Alpine tundra (*Caricetum curvulae*)	Cambic Cryosol
B2m	46° 32′ 40″/9° 48′ 1″	2,648	30	36	Granite/gneiss (Julier Granite)	Alpine tundra (*Caricetum curvulae*)	Cambic Cryosol
B3m	46° 32′ 39″/9° 48′ 2″	2,663	30	30	Granite/gneiss (Julier Granite)	Alpine tundra (*Caricetum curvulae*)	Cambic Cryosol
Albula							
A1m	46° 34′ 32″/9° 53′ 14″	2,620	70	62	Granite/gneiss (Julier Granite)	Alpine tundra (*Caricetum curvulae*)	Cambic Cryosol
A2m	46° 34′ 31″/9° 53′ 16″	2,620	55	62	Granite/gneiss (Julier Granite)	Alpine tundra (*Caricetum curvulae*)	Cambic Cryosol
A3m	46° 34′ 30″/9° 53′ 16″	2,616	50	70	Granite/gneiss (Julier Granite)	Alpine tundra (*Caricetum curvulae*)	Cambic Cryosol
Permafrost sites: subalpine							
Spinas							
S1m	46° 33′ 19″/9° 51′ 29″	1,820	20	57	Granite-rich slope deposits	Natural forest (*Larici-Pinetum cembrae*)	Haplic Cambisol (Dystric)
S2m	46° 33′ 19″/9° 51′ 29″	1,820	20	57	Granite-rich slope deposits	Natural forest (*Larici-Pinetum cembrae*)	Haplic Cambisol (Dystric)
S3m	46° 33′ 18″/9° 51′ 33″	1,808	40	46	Granite-rich slope deposits	Natural forest (*Larici-Pinetum cembrae*)	Haplic Cambisol (Dystric)
S4m	46° 33′ 17″/9° 51′ 33″	1,809	40	53	Granite-rich slope deposits	Natural forest (*Larici-Pinetum cembrae*)	Haplic Podzol

[a] World Geodetic System (WGS84)

[b] IUSS Working Group WRB (2007)

a FLASH Elemental Analyzer 1112 (Thermo Finnigan, Milan, Italy) combined with a CONFLO III Interface (Thermo Finnigan, Bremen, Germany) following standard processing techniques. The stable isotope ratios are reported as $\delta^{13}C$ values [‰] relative to V-PDB defined in terms of NBS 19=1.95‰. The accuracy of

Table 2 Mean ground surface temperature (°C) in the active layer at the Val Bever sites, January–December 2012

	January	February	March	April	May	June	July	August	September	October	November	December	Year
Non-permafrost	−0.5	−1.4	−0.6	0.0	0.2	5.5	10.7	12.0	7.3	3.6	0.6	0.4	3.1
Permafrost	−4.4	−6.3	−4.2	−2.5	0.0	5.7	10.1	10.8	5.5	1.6	0.2	−0.1	1.4

the $^{13}C/^{12}C$ ratio was monitored by analyses of the international standard NBS 22 and an in-house standard INTC, which yielded values of −29.73±0.06‰ (1 standard deviation (SD), n=62) and −35.27±0.05‰ (1 SD, n=62), respectively, during the course of this study. The long-term reproducibility for all standards is better than 0.1‰.

2.8 Conversion of ^{137}Cs and $^{239+240}$Pu activities into soil redistribution rates

^{137}Cs and $^{239+240}$Pu inventories (Bq/m^2) were calculated based on the following equation:

$$As = \frac{1}{S}\sum_i M_{Ti}C_i \quad (1)$$

Where C_i = activity of the ith sub-sample depth increment (Bq/kg), M_{Ti} = total mass of the ith sample depth increment (kg) and S = area of the horizontal core cross (m^2). Soil redistribution rates were calculated by comparing the isotope inventory for an eroding point with a local reference inventory where neither erosion nor soil accumulation is expected. Two different models were used to convert ^{137}Cs and $^{239+240}$Pu inventories into soil redistribution rates:

1. The profile distribution model (PDM) published by Walling and Quine (1990) and Zhang et al. (1990):

$$A'(x) = A_{ref}\left(1-e^{x/h_0}\right) \quad (2)$$

where $A'(x)$ = amount of isotope inventory above depth x (Bq/m^2), x = depth from soil surface expressed as mass between top and actual depth (kg/m^2), A_{ref} = reference inventory as mean of all reference sites (Bq/m^2) and h_0 = profile shape factor (kg/m^2) that is a coefficient describing the rate of exponential decrease in inventory with depth, for soil profiles in uncultivated sites.

The erosion rate Y for a point of interest can be calculated according to equation:

$$Y = \frac{10}{t-t_0} \times \ln\left(1-\frac{X}{100}\right) \times h_0 \quad (3)$$

Y = erosion rate (t/ha/year), t = year of sampling, t_0 = '1986' (year of the Chernobyl nuclear power plant accident; for calculations using ^{137}Cs) or '1963' (thermonuclear weapon testing; for calculations using $^{239+240}$Pu), X = % reduction of total inventory (A_u [Bq/m^2]) in regard to the local reference value $(A_{ref}-A_u)/A_{ref}\times 100$).

2. The inventory method (IM) according to Lal et al. (2013):

$$L = -\frac{1}{\alpha P}\ln\left(1-\frac{I_{loss}}{I_{Ref}}\right) \quad (4)$$

with L = loss of soil, $I_{loss} = I_{ref}-I$, I_{ref}=the local reference inventory as mean of all reference sites (Bq/m^2), I = measured total inventory at the sampling point (Bq/m^2) and P = particle size correction factor, where P>1. Calculations were done using a P factor of 1, 1.2 (according to Walling and He 1999) and 1.5 (according to Lal et al. 2013). Following the approach of Alewell et al. (2013), the coefficient α was obtained from a least squared exponential fit of the isotopes (^{137}Cs and $^{239+240}$Pu) depth profile.

2.9 Conversion of meteoric ^{10}Be in soil redistribution rates

Knowing the age of landform from independent dating (Suter 1981; Böhlert et al. 2011) derived from soils, soil erosion can be estimated by comparing the effective abundance of ^{10}Be measured in the soil with the theoretically necessary abundance for the expected age. The theoretical abundance of ^{10}Be was calculated for an expected soil age of 11 kyears for the alpine Val Bever sites, 8 kyears for the alpine Albula sites and 16 kyears for the subalpine Spinas sites, respectively (Suter 1981; Böhlert et al. 2011). To evaluate a possible erosion of the soils, we assume that the material is eroded from the surface at a constant rate E (Maejima et al. 2005) according to Eq. 5:

$$t_{corr} = -\frac{1}{\lambda}\ln\left(1-\lambda\frac{N}{q-\rho Em}\right) \quad (5)$$

where m = measured concentration of ^{10}Be in the top eroding horizons (atoms/g), E = erosion rate, ρ = the bulk density (g/cm^3) of the top horizons (mean values), N = ^{10}Be inventory of the profile, q = annual deposition rate (calculated according to Monaghan et al. 1985/1986; Brown et al. 1989; Maejima et al. 2005), λ = decay constant of ^{10}Be (4.997×10^{-7}/year) and t_{corr} = correct (expected) age. The apparent age t is given by

$$t = -\frac{1}{\lambda}\ln\left(1-\lambda\frac{N}{q}\right) \quad (6)$$

Erosion or accumulation rates are obtained from the difference $\Delta t = t_{corr} - t$.

3 Results

3.1 General soil properties

All soils were acidic and the pH ranged from about 3.8 in the topsoil up to 4.6 in the deeper soil horizons (Table 3). The lower horizons and parent material consisted of loamy sand to sandy loam, whereas in the topsoil a higher silt and clay content could be measured. Rather well-developed soil profiles, even at very high altitudes (around 2,700 m asl) were found with a relatively high content of soil organic matter at both types of sites (permafrost/non-permafrost; Table 3). Average bulk densities and skeleton contents for the Val Bever sites are given in Table 4, with permafrost soils showing higher bulk densities and skeleton contents than the non-permafrost soils.

3.2 Comparison of ^{137}Cs and $^{239+240}$Pu inventories

At the reference site, ^{137}Cs inventories ranged from 2,243 to 4,075 Bq/m^2 (data not shown) with an average value of 3,139 Bq/m^2 (coefficient of variation CV=21.7 %) (Table 5). The permafrost sites showed ^{137}Cs values from 1,112 to 9,259 Bq/m^2 with a mean of 3,852 Bq/m^2 (CV=69.1 %). The ^{137}Cs inventory of the non-permafrost sites varied between 2,324 and 5,473 Bq/m^2, showing an average of 4,374 Bq/m^2 (CV=22.5).

The $^{239+240}$Pu inventories at the reference site varied between 78 and 104 Bq/m^2 (data not shown), with a mean value of 92 Bq/m^2 (CV=11) (Table 5). The permafrost sites achieved a $^{239+240}$Pu inventory of 32 to 173 $^{239+240}$Pu, with a mean of 80 Bq/m^2 (CV=58). The non-permafrost soils had a $^{239+240}$Pu inventory of 98 to 551 Bq/m^2, with an average of 246 Bq/m^2 (CV=75).

The vertical distribution of ^{137}Cs and $^{239+240}$Pu in the undisturbed reference sites and the adjacent permafrost and non-permafrost sites was similar (Fig. 2). Most of the ^{137}Cs and $^{239+240}$Pu was accumulated in the upper depth intervals and exponentially decreased with increasing soil depth. The variability was the highest in the topsoil increments. At the reference site, the highest amount of radionuclides was present in the upper 3 cm (^{137}Cs 94 %; $^{239+240}$Pu 82 %) (Table 6). In the first 6 cm, the permafrost sites contained 95 % (^{137}Cs) and 88 % ($^{239+240}$Pu) and the non-permafrost sites 92 % (^{137}Cs) and 91 % ($^{239+240}$Pu), respectively. Below 9 cm, no more ^{137}Cs was detected with the exception of the permafrost sites. In contrast, $^{239+240}$Pu was found to a greater soil depth (0–15 cm) at all sites.

3.3 Medium-term soil erosion rates (^{137}Cs and $^{239+240}$Pu)

By applying the PDM (Table 5) to the ^{137}Cs data, most of the permafrost soil cores indicated soil erosion with rates ranging from 15 to 135 t/km^2/year. However, three permafrost soil cores accumulated soil material with 68, 70 and 141 t/km^2/year. For non-permafrost soils, accumulation rates of 34–72 t/km^2/year were achieved. One single non-permafrost soil core showed a soil erosion rate of 39 t/km^2/year. Calculations using the IM (Table 5) showed for permafrost soil cores soil erosion rates of 47–326 t/km^2/year (P=1), 39–271 t/km^2/year (P=1.2) and 31–217 t/km^2/year (P=1.5), respectively. Again, three permafrost soil cores accumulated soil within a range of 156–346 t/km^2/year (P=1), 130–288 t/km^2/year (P=1.2) and 104–231 t/km^2/year (P=1.5), respectively. Non-permafrost sites accumulated soil with 44–88 t/km^2/year (P=1), 37–73 t/km^2/year (P=1.2) and 29–59 t/km^2/year (P=1.5). One single soil core showed erosion rates of 53 t/km^2/year (P=1), 44 t/km^2/year (P=1.2) and 35 t/km^2/year (P=1.5), respectively. Applying the PDM (Table 5) to the $^{239+240}$Pu data, most of the permafrost soils showed erosion rates of 14–120 t/km^2/year. Three permafrost soil cores accumulated soil material with a rate of 2, 23 and 72 t/km^2/year, respectively. Non-permafrost soils showed accumulation rates of 7–204 t/km^2/year. When choosing the IM, soil erosion rates in permafrost soils ranged from 93 to 769 t/km^2/year (P=1), 77 to 641 t/km^2/year (P=1.2) and 62 to 512 t/km^2/year (P=1.5), respectively. Three permafrost soil cores showed accumulation instead of erosion; accumulation rates were ranging from 0 to 322 t/km^2/year (P=1), 10 to 269 t/km^2/year (P=1.2) and 8 to 215 t/km^2/year (P=1.5), respectively. In non-permafrost soils accumulation rates of 20–486 t/km^2/year (P=1), 16–405 t/km^2/year (P=1.2) and 13–324 t/km^2/year (P=1.5) were obtained. Permafrost sites were situated at lower slopes and had a different vegetation cover compared to the non-permafrost sites (Figs. 3 and 4).

3.4 Long-term soil erosion rates (meteoric ^{10}Be)

^{10}Be concentrations within the profiles for permafrost and non-permafrost soils at the alpine and subalpine sites are given in Fig. 5. The ^{10}Be concentrations ranged from 1 to 8 atoms/g×E+8. Non-permafrost soils showed higher ^{10}Be concentrations than permafrost soils; only at the alpine Albula site, the concentrations were moderately comparable in both profile types (permafrost and non-permafrost). The highest ^{10}Be concentrations were found in the topsoil layers and steadily decreased with increasing soil depth.

According to the ^{10}Be method, no clear discernible patterns of the long-term soil erosion rates between permafrost and

Table 3 Physical and chemical characteristics of the fine earth (<2 mm)

Site	Horizon	Depth (cm)	Sand (g/kg)	Silt (g/kg)	Clay (g/kg)	pH ($CaCl_2$)	C_{org} (g/kg)	N (g/kg)	C/N
Non-permafrost sites: alpine									
Val Bever									
B1o	O	0–10	122	577	301	4.0	197	15	13
	OE	10–30	565	197	238	4.0	85.4	7.4	12
	Bs	30–50	760	214	26	4.3	25.9	3.4	8
	C	50–75	875	111	14	4.4	18.2	2.4	8
B2o	A	0–10	–	–	–	4.1	99.3	7.7	13
	AC	10–30	–	–	–	4.1	63.5	6.2	10
	bA	30–50	–	–	–	4.3	47.8	5.0	10
	R	>50	–	–	–	–	–	–	–
B3o	O	0–10	–	–	–	3.9	110.0	7.8	14
	AE	10–30	–	–	–	4.1	107.0	7.1	15
	Bhs	30–50	–	–	–	4.3	42.2	3.6	12
	Bs	50–60	–	–	–	4.5	13.7	2.3	6
	C	60–70	–	–	–	4.6	6.1	1.4	4
Albula									
A1o	AE	0–10	483	341	176	3.8	33.0	3.0	11
	BA	10–20	448	371	180	4.1	15.9	2.3	7
	Bhs1	20–40	485	345	170	4.1	15.0	2.1	7
	Bhs2	40–60	723	224	52	4.4	27.9	1.9	15
	C	60–70	653	305	42	4.5	10.9	0.2	50
A2o	AE	0–10	–	–	–	3.8	73.9	5.5	13
	Bhs1	10–20	–	–	–	4.4	39.8	4.1	10
	Bhs2	20–35	–	–	–	4.2	14.8	2.8	5
	C	35–45	–	–	–	4.5	8.7	1.6	5
A3o	A	0–10	–	–	–	3.5	79.6	7.4	11
	AE	10–20	–	–	–	3.8	43.6	5.1	9
	Bh1	20–40	–	–	–	4.2	32.3	3.6	9
	Bh2	40–60	–	–	–	4.3	29.2	3.1	9
	C	60–75	–	–	–	4.5	13.5	2.5	5
Non-permafrost sites: subalpine									
Spinas									
S1o	E	0–10	728	205	67	4.0	58.4	3.2	18
	Bs1	10–20	750	214	36	3.4	49.9	3.8	13
	Bs2	20–30	749	220	31	4.3	37.7	2.2	18
	Bs3	30–40	778	184	38	4.4	35.1	2.7	13
	B	50–60	649	233	118	4.4	31.9	2.7	12
	R	>60	–	–	–	–	–	–	–
S2o	E	0–10	–	–	–	3.8	63.5	5.8	11
	Bs1	10–20	–	–	–	4.2	31.0	3.4	9
	Bs2	40–50	–	–	–	4.5	19.8	2.3	9
	B	70–80	–	–	–	4.4	15.8	2.4	7
	R	>80	–	–	–	–	–	–	–
S3o	A	0–10	–	–	–	3.8	65.7	3.2	21
	E	10–20	–	–	–	3.8	91.5	3.7	25
	Bh1	20–30	–	–	–	3.7	151.5	4.5	34
	Bh2	30–40	–	–	–	3.7	130.0	4.1	32
	IIE	40–50	–	–	–	3.7	25.3	1.2	21
	Bs	60–100	–	–	–	4.6	29.2	0.7	42
	R	>100	–	–	–	–	–	–	–

Table 3 (continued)

Site	Horizon	Depth (cm)	Sand (g/kg)	Silt (g/kg)	Clay (g/kg)	pH ($CaCl_2$)	C_{org} (g/kg)	N (g/kg)	C/N
Permafrost sites: alpine									
Val Bever									
B1m	A	0–10	793	130	77	4.5	15.8	3.1	5
	Bw1	10–30	848	89	63	4.5	12.8	2.2	6
	Bw2	30–50	786	133	81	4.5	20.1	2.6	8
	BC	50–60	814	103	83	4.6	11.6	2.1	6
	R	>60	–	–	–	–	–	–	–
B2m	Ah	0–10	589	295	117	4.6	19.6	3.1	6
	Bw1	10–30	688	224	88	4.6	12.1	2.6	5
	Bw2	30–35	–	–	–	4.6	12.6	1.9	7
	Bw3	35–50	656	262	82	4.6	14.9	2.5	6
	C	50–80	587	301	113	4.6	12.7	2.3	5
B3m	Ah	0–10	–	–	–	4.4	29.6	3.8	8
	Bw	10–30	–	–	–	4.6	11.5	2.7	4
	BC1	30–50	–	–	–	4.7	7.2	1.7	4
	BC2	50–60	–	–	–	4.7	6.1	2.0	3
	R	>60	–	–	–	–	–	–	–
Albula									
A1m	A1	0–10	543	293	164	3.9	27.4	2.3	12
	A2	10–20	512	332	156	4.0	20.8	1.8	12
	AE	20–40	524	313	163	4.1	21.4	1.3	16
	Bs	40–80	619	272	109	4.6	22.1	1.2	18
	BC	80–100	674	277	49	4.3	6.6	0.3	26
	R	>100	–	–	–	–	–	–	–
A2m	AE1	0–10	–	–	–	3.6	71.2	4.1	18
	AE2	10–20	–	–	–	3.9	42.2	3.8	11
	Bhs	20–45	–	–	–	4.3	20.4	1.7	12
	B	45–80	–	–	–	4.5	10.3	2.4	4
	C	80–100	–	–	–	4.6	3.6	0.2	17
A3m	A	0–10	–	–	–	3.8	96.4	5.6	17
	AE1	10–20	–	–	–	3.9	63.6	3.8	17
	AE2	20–35	–	–	–	4.1	55.6	2.7	21
	Bhs	35–60	–	–	–	4.5	32.3	1.4	23
	C	60–70	–	–	–	4.6	9.8	0.2	42
Permafrost sites: subalpine									
Spinas									
S1m	A	0–10	633	218	149	3.8	40.0	4.3	9
	Bw	25–35	611	239	150	4.4	21.3	2.5	9
	BC	50–60	622	234	144	4.5	21.3	2.4	9
	R	>60	–	–	–	–	–	–	–
S2m	A	0–10	–	–	–	3.9	64.4	3.5	18
	Bw	25–35	–	–	–	4.1	45.2	2.2	21
	BC	50–60	–	–	–	4.1	49.0	2.4	20
	R	>60	–	–	–	–	–	–	–
S3m	Ah	0–10	–	–	–	3.5	93.2	5.5	17
	Bw1	10–20	–	–	–	4.0	36.6	3.0	12
	Bw2	20–30	–	–	–	4.1	32.6	3.0	11
	BC1	30–40	–	–	–	4.2	33.2	2.8	12
	BC2	40–50	–	–	–	4.3	29.3	2.1	14
	C	50–60	–	–	–	4.3	33.1	3	11

Table 3 (continued)

Site	Horizon	Depth (cm)	Sand (g/kg)	Silt (g/kg)	Clay (g/kg)	pH ($CaCl_2$)	C_{org} (g/kg)	N (g/kg)	C/N
S4m	AE	0–10	–	–	–	3.9	57.4	2.1	27
	Bh	10–20	–	–	–	3.9	35.8	0.8	45
	Bhs1	20–30	–	–	–	4.2	34.3	1.1	31
	Bhs2	30–40	–	–	–	4.3	39.9	0.7	57
	Bhs3	40–50	–	–	–	4.3	33.0	0.2	165
	Bhs4	50–60	–	–	–	4.3	40.5	0.8	51
	Bs1	60–70	–	–	–	4.3	36.8	0.8	46
	Bs2	70–90	–	–	–	4.3	20.9	0.6	35
	R	>90	–	–	–	–	–	–	–

non-permafrost soils could be measured (Table 7). In general, the soil redistribution rates were low (erosion rates up to 49 t/km^2/year or 41 mm/kyear and accumulation rates up to 4 t/km^2/year or 4 mm/kyear).

3.5 δ^{13}C as indicator for disturbance processes

The values of the reference site increased with depth from −25 to −23‰ at the Val Bever reference site and from −25 to −24 ‰ at the Albula reference site (data not shown). A positive correlation between the total carbon content and δ^{13}C value was obtained for the undisturbed reference soil at the Val Bever (R^2=0.63) and the Albula reference site (R^2=0.65) (Fig. 6). In contrast, the non-permafrost soils and the permafrost soils at the Val Bever site showed very low correlations between organic carbon and δ^{13}C values (R^2=0.17 and R^2=0.04, respectively). Comparable low correlations were found at the Albula site (non-permafrost: R^2=0.20; permafrost: R^2=0.15).

Table 4 Physical characteristics of the investigated soils in 0–15 cm soil depth at the Val Bever sites (for the analysis of short-term erosion rates using ^{137}Cs and $^{239+240}$Pu)

Site	Soil depth (cm)	Skeleton[a] >2 mm (wt%)	Bulk density[a] (g/cm^3)
Reference	0–3	19±13	0.40±0.2
	3–6	43±17	0.91±0.2
	6–9	35±8	1.00±0.2
	9–12	36±24	1.24±0.2
	12–15	35±17	1.16±0.1
Non-permafrost	0–3	10±17	0.22±0.1
	3–6	16±20	0.42±0.1
	6–9	21±23	0.45±0.1
	9–12	18±34	0.44±0.1
	12–15	16±36	0.48±0.2
Permafrost	0–3	35±21	0.52±0.2
	3–6	34±25	0.84±0.3
	6–9	31±17	0.84±0.2
	9–12	43±19	0.96±0.3
	12–15	44±20	0.88±0.3

[a] Shown are average values for reference, non-permafrost and permafrost soils at the Val Bever sites

4 Discussion

4.1 Medium-term soil erosion rates (^{137}Cs and $^{239+240}$Pu)

The choice of an adequate calculation procedure is essential for the quantification of soil erosion rates. The profile distribution model (PDM) resulted in lower soil redistribution rates compared to the inventory method (IM). Compared to other fallout radionuclide (FRN)-based soil erosion rates in mountain environments, the erosion rates measured in this study were considerably lower. For example, Konz et al. (2009, 2010) and Ceaglio et al. (2012) determined with the ^{137}Cs method yearly soil redistribution rates from 500 to >3,000 t/km^2 for Swiss and Italian alpine soils, respectively. Alewell et al. (2013) evaluated soil redistribution rates of 2,000 t/km^2/year erosion to 2,500 t/km^2/year of deposition for two alpine valleys. Avalanches, snow gliding and other winter-related processes combined with more or less intensive land use (grazing and mowing) were responsible for such high rates (Konz et al. 2009; Ceaglio et al. 2012). Our sites, however, were not located within typical avalanche paths and not used for pasture, which might explain the much lower erosion rates. Differences in vegetation cover at permafrost and non-permafrost sites influenced soil redistribution independently from the slope. Vegetation can act as a physical barrier by influencing the particle flow at the surface. They can further protect soil by increasing the infiltration rate (Ziegler and Giambelluca 1998), stabilising the soil with their roots

Table 5 Erosion rates quantified by the ^{137}Cs and $^{239+240}$Pu inventory for the alpine (Val Bever) permafrost and non-permafrost soils. Calculations were done according to the profile distribution model (Walling and Quine 1990; Zhang et al. 1990) and the inventory model (Lal et al. 2013). A particle size correction factor (P) of 1.2 (according to Walling and He 1999) and 1.5 (according to Lal et al. 2013) was included for the inventory method

Site	Inventory (Bq/m^2)		Soil redistribution rate[a] (t/km^2/year)		Soil redistribution rate[b] (t/km^2/year) P=1		Soil redistribution rate[b] (t/km^2/year) P=1.2		Soil redistribution rate[b] (t/km^2/year) P=1.5	
	^{137}Cs	$^{239+240}$Pu	^{137}Cs	$^{239+240}$Pu	^{137}Cs	$^{239+240}$Pu	^{137}Cs	$^{239+240}$Pu	^{137}Cs	$^{239+240}$Pu
Non-permafrost										
B1o1	4,417	257	44	117	54	285	45	238	36	190
B102	5,473	520	72	197	88	486	73	405	59	324
B1o3	5,424	551	71	204	83	480	69	400	55	320
B2o1	4,090	159	34	62	59	176	49	147	39	118
B2o2	4,749	136	54	44	88	145	73	121	58	97
B2o3	4,387	144	43	51	50	118	42	98	33	79
B2o4	4,128	104	36	14	44	36	37	30	29	24
B3o1	2,324	98	−39	7	−53	20	−44	16	−35	13
Permafrost										
B1m1	2,046	32	−56	−120	−176	−769	−147	−641	−118	−512
B1m2	9,259	94	141	2	346	0	288	10	231	8
B2m1	5,303	113	68	23	213	145	177	121	142	97
B2m2	1,112	43	−135	−86	−326	−421	−271	−351	−217	−281
B2m3	2,802	81	−15	−14	−47	−93	−39	−77	−31	−62
B3m1	2,582	43	−25	−86	−79	−544	−66	−454	−53	−363
B3m3	5,394	173	70	72	156	322	130	269	104	215
B3m4	2,319	64	−39	−41	−66	−137	−55	−114	−44	−91
Reference SD	3,139.4±682.2	92.0±10.3								
Non-permafrost SD	4,374.1±985.3	246.0±185.3	39±35	87±78	52±46	218±183	43±38	182±153	34±31	146±122
Permafrost SD	3,852.0±2,660.6	80.4±46.6	1±87	−31±64	3±220	−186±367	2±184	−155±306	2±147	−124±244

Negative values = erosion; positive values = accumulation

[a] Walling and Quine (1990); Zhang et al. (1990)

[b] Lal et al. (2013)

(Gyssels et al. 2005) and reducing the raindrop energy with their canopy (Bochet et al. 1998).

4.2 Distribution and origin of ^{137}Cs and $^{239+240}$Pu

After deposition on the soil surface, the radioisotopes of interest are rapidly adsorbed to soil particles. Nakanishi et al. (2014) observed that the major part of ^{137}Cs in the litter layer moved into the mineral soil within 1 year after the accident of Fukushima. The topsoil prevented migration of ^{137}Cs, and only 2 % of ^{137}Cs in the leachate from litter and humus layer penetrated below a 10-cm depth. The mobility of these isotopes within the soil profile is, however, rather complex and depends on several factors such as the chemistry of the isotopes, organic carbon content, clay mineralogy, cation exchange capacity (CEC) and pH (e.g. Gal et al. 2007; Zhiyanski et al. 2008). Whereas $^{239+240}$Pu is preferentially attached to soil organic matter and sesquioxides (Bunzl et al. 1995), ^{137}Cs is mainly adsorbed by the mineral fraction (especially illitic minerals; Bradbury and Baeyens 2000). It has been demonstrated that ^{137}Cs mobility can be enhanced in organic-rich soils (Staunton et al. 2002), but as shown elsewhere, even organic upland soils contained enough illitic material to immobilize ^{137}Cs (Dumat et al. 1997). A low migration rate of ^{137}Cs and $^{239+240}$Pu is, however, indicated in our investigation by their accumulation within the upper 10 cm, which is typical for undisturbed soils (Kirchner et al. 2009). The greater downward migration (0–15 cm soil depth) of $^{239+240}$Pu has also been reported elsewhere (e.g. Lal et al. 2013) and is due to the timing of the fallout deposits ($^{239+240}$Pu bomb fallout in the 1952 and 1964 compared to the main ^{137}Cs fallout of Chernobyl in 1986).

The fallout radionuclide (FRN) inventories at the reference site varied considerably even on a relatively small scale. For

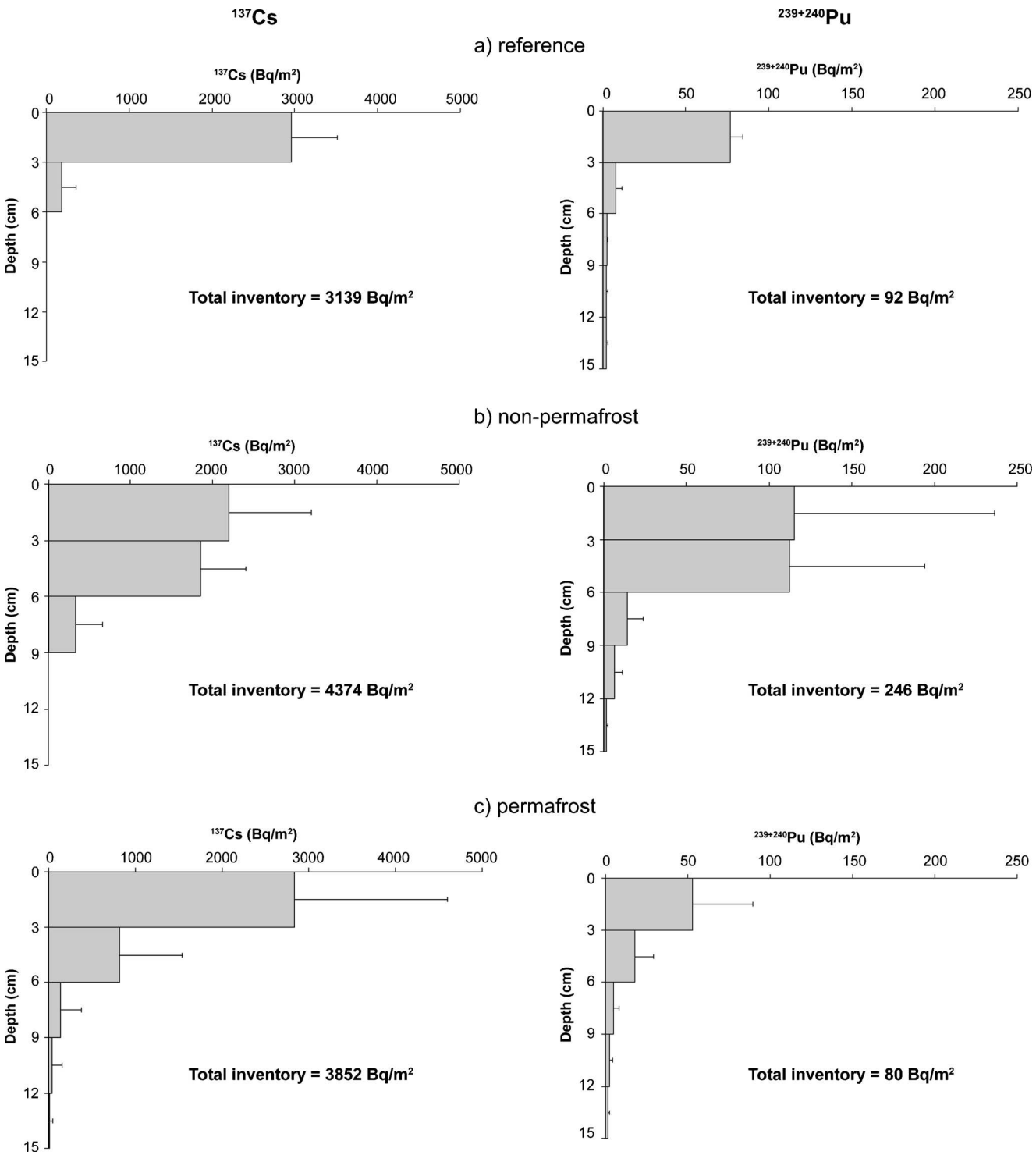

Fig. 2 Activity depth profiles with depth increments at the alpine site 'Val Bever' for ^{137}Cs (*left*) and $^{239+240}$Pu (*right*) together with the corresponding inventory. *Error bars* show the standard deviation

alpine regions in Austria, Lettner et al. (2000) estimated that the intrinsic spatial variability of the fallout accounted for 17.7 % of the observed variability. Differences in soil surface characteristics such as a high skeleton content and vegetation cover might additionally have hindered the isotope deposition on the soil surface. Furthermore, processes such as litter fall, uptake by roots or the loss via subsurface flow can alter the amount of anthropogenic radioisotopes (e.g. ^{137}Cs and $^{239+240}$Pu) that enter the soil system (Voigt and Fesenko 2009). The uptake of radionuclides (e.g. ^{137}Cs, $^{239+240}$Pu) by plants

Table 6 Fractions of $^{239+240}$Pu and ^{137}Cs inventories (Val Bever sites)

Site	Soil depth (cm)	Fraction of total inventory (%)	
		^{137}Cs	$^{239+240}$Pu
Reference	0–3	94	82
	3–6	6	9
	6–9	0	3
	9–12	0	3
	12–15	0	3
Non-permafrost	0–3	50	46
	3–6	42	45
	6–9	8	6
	9–12	0	3
	12–15	0	1
Permafrost	0–3	74	65
	3–6	21	23
	6–9	4	6
	9–12	1	3
	12–15	0	2

depends on several factors such as the availability of competing cations or plant species (Gastberger et al. 2000; Yoshihara et al. 2013). A biological uptake of e.g. ^{137}Cs can be considered relatively low (Rogowski and Tamura 1970) compared to the total amount, although estimates of mass calculations are very rare. Radionuclides adsorbed to plant surfaces or taken up by roots will be washed off or released to soils when the plants die and decompose (Rogowski and Tamura 1970; Dahlman et al. 1975). Ould-Dada (2002) demonstrated that radionuclide releases from nuclear installations showed a complex pattern of deposition within the canopy. A considerable part is already filtered out in the upper part of the canopy

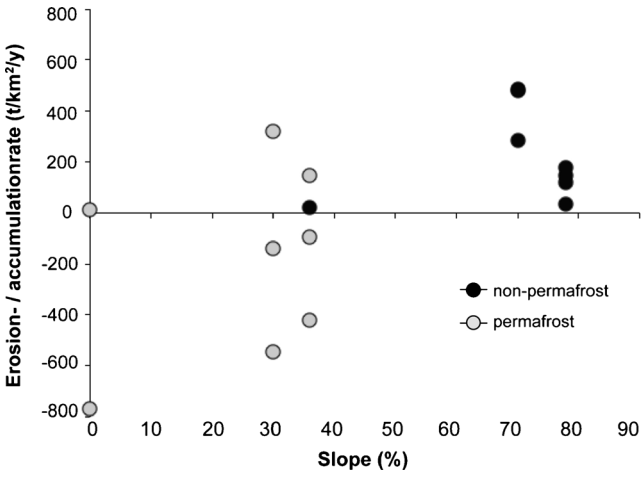

Fig. 3 Comparison of soil redistribution rates (t/km^2/year) with slope for permafrost and non-permafrost soils at the alpine site 'Val Bever'. Soil redistribution rates are based on $^{239+240}$Pu inventories using the inventory method (Lal et al. 2013). Negative values indicate soil erosion

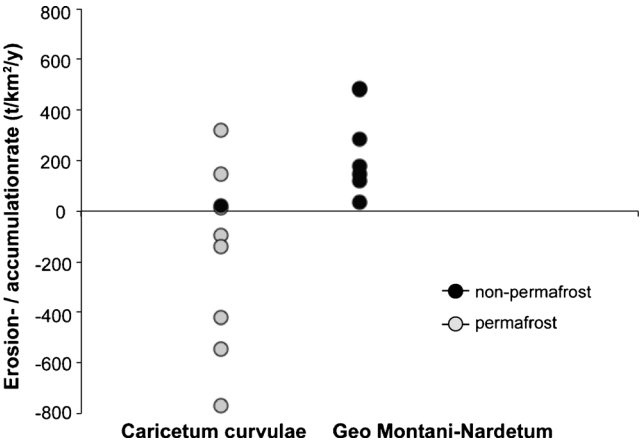

Fig. 4 Soil redistribution rates (t/km^2/year) and vegetation community for permafrost and non-permafrost soils at the alpine site 'Val Bever'. Soil redistribution rates are based on $^{239+240}$Pu inventories using the inventory method (Lal et al. 2013). Negative values indicate soil erosion

layer. However, this should have no effect on the estimate of erosion rates because ^{137}Cs and $^{239+240}$Pu isotope concentrations in the soils are usually related to undisturbed sites having similar environmental conditions. To avoid potential complications, we did not investigate ^{137}Cs and $^{239+240}$Pu isotopes at the subalpine, forested sites.

The greater heterogeneity of the ^{137}Cs inventories at the alpine site Bever might be related to the snow cover, which was still present in April/May during the distribution and deposition of the Chernobyl ^{137}Cs. The snow cover most likely hindered partially the direct adsorption of ^{137}Cs to the soil particles and the ^{137}Cs were then redistributed heterogeneously during snowmelt. An inhomogeneous distribution of ^{137}Cs is furthermore supported by the fact that a ^{137}Cs inventory found in the investigated soils was relatively low (3,139 Bq/m^2, year 2011) compared to an expected inventory ranging between 4,072 and 7,406 Bq/m^2 in the year 2011. The expected inventory of 4,072–7,406 Bq/m^2 is composed of the decay-corrected Chernobyl inventory of 2,252–75,631 Bq/m^2 in the year 2011 (initial inventory in the year 1986, 4,000–10,000 Bq/m^2; De Cort et al. 1998) and the decay-corrected fallout of 1,775 Bq/m^2, which is in the year 2011 still present from nuclear weapon testing (Walling and He 2000). Consequently, only 44 % of the ^{137}Cs were related to the Chernobyl accident, whereas the bomb fallout accounts for 56 % of the inventory. Another indicator of FRN origin is the ^{137}Cs/$^{239+240}$Pu ratio, which shows an average of 43.5 for the upper 3 cm in the investigated soils. Such a value is relatively close to the ^{137}Cs/$^{239+240}$Pu ratio of 36±4 that is characteristic for atomic weapon testing fallout (Turner et al. 2003). Hence, considering the relatively low amount of Chernobyl ^{137}Cs found at the investigated sites, the ^{137}Cs measurements do not explicitly display soil erosion that has occurred after 1986.

In contrast, $^{239+240}$Pu is deposited all year round, which means that 50 % of the $^{239+240}$Pu has the same heterogeneity

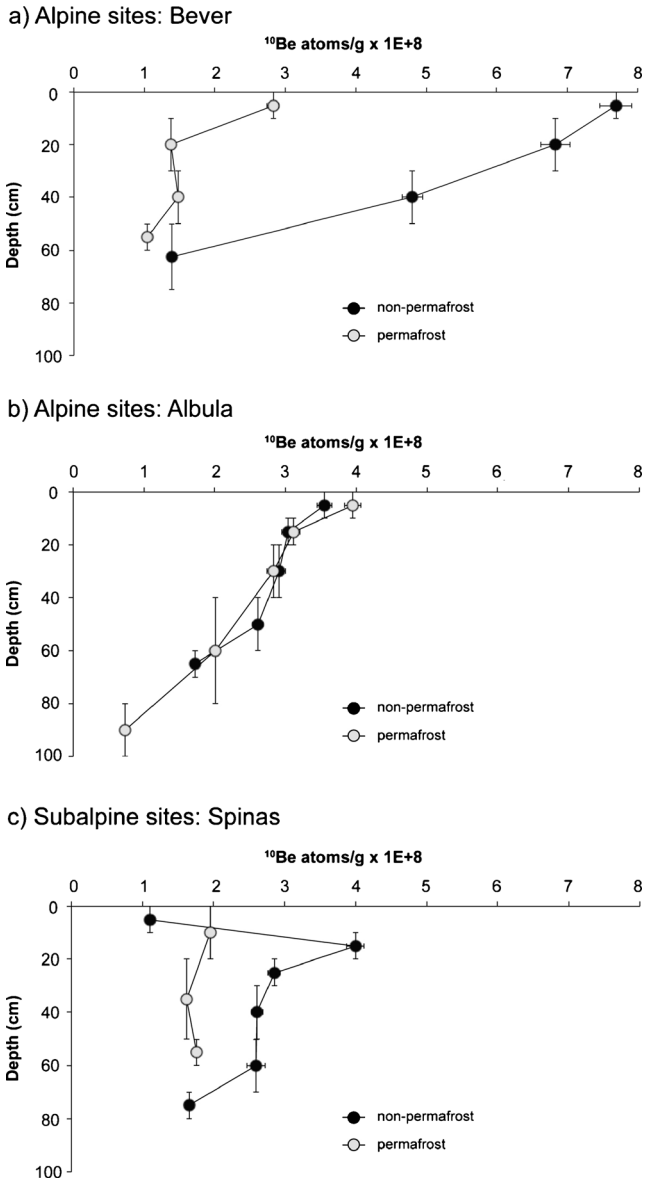

Fig. 5 Depth profiles showing the accumulated meteoric ^{10}Be in the permafrost and non-permafrost soils at the alpine (Val Bever and Albula—**a**, **b**) and subalpine sites (Spinas—**c**). The *vertical bars* indicate the horizon depth range and *horizontal error bars* the standard deviation of the measured values

(winter snow cover), but the rest might be distributed more heterogeneously as rain input. The $^{239+240}$Pu inventory at the reference site was within the range of 50 to 100 Bq/m^2, which is the expected inventory for the northern hemisphere. Additionally, the $^{239+240}$Pu reference inventory corresponds well to the one found in two other alpine valleys (83 and 77 Bq/m^2 for the Ursern Valley and the Val Piora, respectively; Alewell et al. 2013). With a ^{239}Pu/^{240}Pu atom ratio of 0.180±0.014, the $^{239+240}$Pu fallout could further be identified as 'bomb-derived' fallout (Kelley et al. 1999). Thus, the lower spatial variability of $^{239+240}$Pu supports the hypothesis that the Chernobyl ^{137}Cs was not homogeneously distributed over the investigated area. Therefore, soil erosion rates based on ^{137}Cs are less reliable than the one obtained by the $^{239+240}$Pu technique.

Table 7 Long-term soil erosion rates using meteoric ^{10}Be for the alpine (Val Bever and Albula sites) and subalpine (Spinas sites) permafrost and non-permafrost soils. The erosion rates were calculated for an expected soil age of 11 kyears for the alpine 'Val Bever' sites, 8 kyears for the alpine 'Albula' sites and 16 kyears for the subalpine 'Spinas' sites, respectively (Suter 1981)

Site	Long-term soil erosion rates (t/km^2/year) meteoric ^{10}Be[a]
Alpine Bever	
Non-permafrost	3
Permafrost	−44
Alpine Albula	
Non-permafrost	−17
Permafrost	4
Subalpine	
Non-permafrost	−49
Permafrost	−45

Negative values = erosion; positive values = accumulation

4.3 Meteoric ^{10}Be in the soil profiles

^{10}Be concentrations in the profiles for permafrost and non-permafrost soils at the alpine and subalpine sites are consistent with already published data for alpine soils (Egli et al. 2010). Such a 'decline type' of ^{10}Be concentration in the soil profile where most of the meteoric ^{10}Be is concentrated in the uppermost 20 cm is typical for young or rapidly eroding soils with insufficient time for downward transportation (Graly et al. 2010). Retention and depletion of ^{10}Be within the soil profile is driven by transport and translocation mechanisms. It is assumed that soil properties such as soil pH, the occurrence of clay minerals, weakly crystalline oxides, hydroxides and organic matter control these processes to a certain extent (Maejima et al. 2005; Egli et al. 2010). The acidic soil conditions made a downward translocation of clay particles containing adsorbed ^{10}Be rather unlikely, due to a higher solubility of Al^{3+} that has a flocculating effect. Additionally, as the ^{10}Be concentration in our investigated soils follows a 'decline' shape, we have to assume that a substantial loss of ^{10}Be in the upper layers and subsequent allocation into the deeper layers can be neglected.

4.4 Long-term soil erosion rates (meteoric ^{10}Be)

In general, the calculated long-term erosion rates were in the range of already reported values using in situ ^{10}Be. Granger et al. (2001) calculated catchment erosion rates at Adams Peak

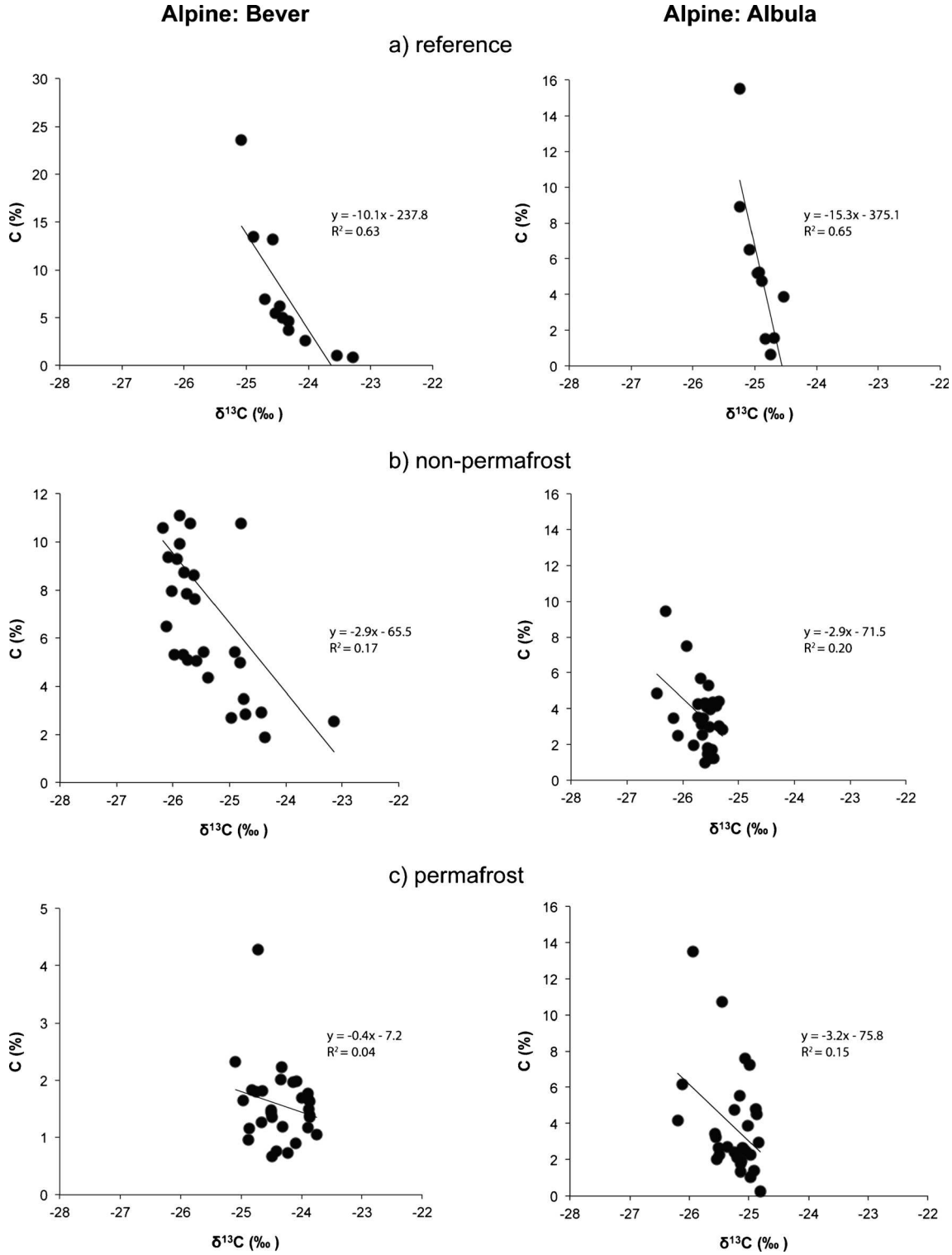

Fig. 6 Correlation between organic carbon content and δ^{13}C-values (as an indicator of potential soil disturbance patterns) for the reference (**a**), non-permafrost (**b**) and permafrost (**c**) soils at the alpine sites 'Val Bever' and 'Albula'

and Antelope Lake (north-eastern Sierra Nevada, CA, USA) of 15–60 mm/kyear. Schaller et al. (2001) showed erosion rates of 20–100 mm/kyear for middle European river catchments.

However, the results for the permafrost and non-permafrost soils were inconsistent between the different sites. Whereas permafrost soils experienced soil loss at the alpine 'Val Bever' site, such soil accumulated material at the alpine 'Albula' site

on very low rates. At the subalpine range, both soils (permafrost and non-permafrost) showed relatively similar erosion rates. These findings can be related to comparable site factors at the subalpine sites such as slope, vegetation or aspect, whereas sites at the alpine level differ in those parameters. Another explanation for the inconsistent results, especially at the alpine sites, might be attributed to the soil formation and landscape evolution in alpine environments, which was not always straightforward. Since the onset of the Holocene (11,000 years BP), warmer and cooler periods influenced soil processes (Haas et al. 1998; Maisch 2001; Davis et al. 2003; Böhlert et al. 2011). A thermal maximum was reached during the Holocene thermal optimum (8–5 kyears BP) when summer temperatures were about 1.5 to 3 °C higher compared to the present-day situation (Davis et al. 2003). The opposite extreme was recorded for the Little Ice Age (AD 1850) when temperatures decreased about 1.5 °C to present values (Filippi et al. 1999). It is therefore highly possible that nowadays permafrost and non-permafrost soils have already been subject to different freeze-thaw processes in the past. An inconsistent permafrost distribution during the last millennia might have been the cause for the differences in long-term redistribution rates on permafrost and non-permafrost at the alpine Val Bever and Albula sites.

By comparing medium- (cf. Section 3.3) and long-term soil erosion rates, it seems that the medium-term soil redistribution rates are in general higher and in part even distinctly higher than the long-term rates. At the Val Bever site, both erosion and accumulation rates seemed to have increased during the last few decades. This statement is still slightly speculative, because the question whether these changes are now really due to a recent increase of the process rates or maybe due to methodological inherences cannot be fully answered. We nonetheless hypothesise that soil redistribution rates in such high-alpine areas have started to increase.

Consequently, the effects of climate warming on subsurface soil conditions (permafrost melting) might be one out of several explanatory factors for the observed increase in medium-term soil redistribution rates (indicated by the $^{239+240}$Pu method). Additional processes (and related changes) exist that may have played a significant role in soil removal such as wind erosion and surface runoff after snowmelt and heavy rainfall events within the last decades. With climate warming, these processes might probably even more change in intensity and frequency with major consequences on soil erosion magnitude.

4.5 δ^{13}C as indicator of disturbance processes

The δ^{13}C signature in topsoil layers showed values within the typical range of C_3 plants (−20 to −30‰) (Kohn 2010). For undisturbed oxic soils, a correlation between the decreasing soil organic carbon (SOC) content and an increasing δ^{13}C with soil depth is expected (Schaub and Alewell 2009). A slightly increasing δ^{13}C value with soil depth was recorded for the reference sites. This relatively low enrichment of 1 to 2‰ in the carbon isotopic signature is typical for either young soils with little time for soil formation or soils with reduced decomposition and thus limited fractionation (Schaub and Alewell 2009; Alewell et al. 2011). The carbon content and δ^{13}C signature in the Val Bever and Albula reference soil were positively correlated, indicating an undisturbed soil development. At the Val Bever site, it seems that the non-permafrost soils were less disturbed (R^2=0.17) than the adjacent permafrost soils (R^2=0.04). The scarcer vegetation in the topsoil makes the permafrost soils probably more prone to erosion. Cryoturbation may also contribute to a rather disturbed δ^{13}C. Cryogenesis is often the controlling factor in patterned ground formation resulting in cryoturbated soil profiles, cryostructures and carbon sequestration (Ping et al. 2008). At the Albula site, however, both soil types (non-permafrost and permafrost) showed a similar SOC and δ^{13}C pattern. Most interestingly, even though net soil redistribution rates indicated by the various methods are rather low, with the δ^{13}C technique, sites affected by soil redistribution and undisturbed reference sites could clearly be separated. Thus, the correlation between δ^{13}C signature and carbon content of a soil profile seems to be a sensitive, qualitative indicator for soil disturbances.

5 Conclusions

Soils with and without permafrost conditions at subalpine and alpine levels with respect to their erosion behaviour using different isotope techniques have been compared. We obtained the following main findings:

Medium-term soil erosion (^{137}Cs and $^{239+240}$Pu):

- Methodological problems were encountered when using ^{137}Cs as erosion tracer: a significant part of the deposited ^{137}Cs that was derived from the Chernobyl accident seemed to be washed out directly after deposition during the snowmelt period (without being incorporated into the soils). Consequently, this method does not seem to be appropriate in high-alpine regions that were snow-covered during the Chernobyl fallout. Only about 44 % of the detected ^{137}Cs could be attributed to the Chernobyl accident.
- $^{239+240}$Pu showed a more homogenous distribution when compared to ^{137}Cs. Consequently, $^{239+240}$Pu is more suitable as a soil erosion tracer (in Chernobyl ^{137}Cs-affected areas).
- $^{239+240}$Pu measurements indicated that permafrost soils rather exhibited erosion, whereas non-permafrost soils accumulated material on the medium term. Although

some sites had relatively steep slopes, a dense vegetation cover led to an accumulation of soil by better stabilising the soil.

Soil disturbance indicator $\delta^{13}C$:

– The $\delta^{13}C$ signature is a valuable tool for indicating disturbance patterns even in high-alpine soils. However, no quantification of erosion is possible.

Long-term soil erosion using meteoric ^{10}Be:

– Relatively low redistribution rates were obtained over the whole soil formation period, with no clear discernible patterns between permafrost and non-permafrost soils. Alternating warmer and cooler periods during the Holocene seemed to influence soil evolution and partially over-shadowed the effect of permafrost on soil characteristics.

According to our findings, soil redistribution rates have increased during the last few decades. The question whether this is now due to climate change and related accelerated geomorphodynamic processes in high-alpine environments or rather due to methodological inaccuracies cannot be fully answered. Furthermore, the findings were not always equivocal and demonstrate that alpine soils have had a complex genesis. Soil formation and also permafrost distribution were not continuous or progressive as they were affected by alternating warmer and cooler conditions since the beginning of the Holocene. A time-split approach using natural and anthropogenic radionuclides as well as stable isotopic signature of δ^{13} C seems to be promising to decipher accelerated soil erosion caused by climate change.

Acknowledgments This research was supported by the Swiss National Foundation (SNF) project grant no. 200021M_134479.

References

Alewell C, Meusburger K, Brodbeck M, Bänninger D (2008) Methods to describe and predict soil erosion in mountain regions. Landsc Urban Plan 88:46–53

Alewell C, Giesler R, Klaminder J, Leifeld J, Rollog M (2011) Stable carbon isotopes as indicators for environmental change in palsa peats. Biogeosciences 8:1769–1778

Alewell C, Meusburger K, Juretzko G, Mabit L, Ketterer ME (2013) Suitability of $^{239+240}Pu$ and ^{137}Cs as tracers for soil erosion assessment in mountain grasslands. Chemosphere. doi:10.1016/j.chemosphere.2013.12.016

Bochet E, Rubio JL, Poesen J (1998) Relative efficiency of three representative matorral species in reducing water erosion at the microscale in a semi-arid climate. Geomorphology 23:139–150

Böckli L, Brenning A, Gruber S, Noetzli J (2012) A statistical approach to modelling permafrost distribution in the European Alps or similar mountain ranges. Cryosphere 6:125–140

Böhlert R, Egli M, Maisch M, Brandová D, Ivy-Ochs S, Kubik PW, Haeberli W (2011) Application of a combination of dating techniques to reconstruct the Lateglacial and early Holocene landscape history of the Albula region (eastern Switzerland). Geomorphology 127:1–13

Bradbury MH, Baeyens B (2000) A generalised sorption model for the concentration dependent uptake of caesium by argillaceous rocks. J Contam Hydrol 42:141–163

Brown L, Stensland GJ, Klein J, Middleton R (1989) Atmospheric deposition of ^{7}Be and ^{10}Be. Geochim Cosmochim Acta 53:135–142

Bunzl K, Flessa H, Kracke W, Schimmack W (1995) Association of fallout $^{239+240}Pu$ and ^{241}Am with various soil components in successive layers of a grassland soil. Environ Sci Technol 29:2513–2518

Ceaglio E, Meusburger K, Freppaz M, Zanini E, Alewell C (2012) Estimation of soil redistribution rates due to snow cover related processes in a mountainous area (Valle d'Aosta, NW Italy). Hydrol Earth Syst Sci 16:517–528

Dahlman RC, Francis CW, Tamura T (1975) Radiocesium cycling in vegetation and soil. In: Howell FG, Gentry JB, Smith MH (eds) Mineral cycling in southeastern ecosystems. USAEC Symposium Series, CONF-740513. US Atomic Energy Commission, Washington, pp 462–481

Davis BAS, Brewer S, Stevenson AC, Guiot J, data contributors (2003) The temperature of Europe during the Holocene reconstructed from pollen data. Quat Sci Rev 22:1701–1716

De Cort M, Dubois G, Fridman ShD, Germenchuk MG, Izrael YuA, Janssens A, Jones AR, Kelly GN, Kvasnikova EV, Matveenko II, Nazarov IM, Pokumeiko YuM, Sitak VA, Stukin ED, Tabachny LYa, Tsaturov YuS, Avdyushin SI (1998) Atlas of caesium deposition on Europe after the Chernobyl accident. Available via ECJRC. http://rem.jrc.ec.europa.eu/RemWeb/Browse.aspx?path=Atlas. Accessed 03 Feb 2014

Dumat C, Cheshire MV, Fraser AR, Shand CA, Staunton S (1997) The effect of removal of soil organic matter and iron on the adsorption of radiocaesium. Eur J Soil Sci 48:675–683

Egli M, Brandova D, Böhlert R, Favilli F, Kubik PW (2010) ^{10}Be inventories in Alpine soils and their potential for dating land surfaces. Geomorphology 119:62–73

Everett SE, Tims SG, Hancock GJ, Bartlwy R, Fifield LK (2008) Comparison of Pu and ^{137}Cs as tracers of soil and sediment transport in a terrestrial environment. J Environ Radioact 99:383–393

Filippi ML, Lambert P, Hunziker J, Kubler B, Bernasconi S (1999) Climatic and anthropogenic influence on the stable isotope record from bulk carbonates and ostracodes in Lake Neuchatel, Switzerland, during the last two millennia. J Paleolimnol 21:19–34

Freppaz M, Godone D, Filippa G, Maggioni M, Lunardi S, Williams MW, Zanini E (2010) Soil erosion caused by snow avalanches: a case study in the Aosta Valley (NW Italy). Arct Antarct Alp Res 42:412–421

Gal JF, Maria PC, Massi L, Mayeux C, Burk P, Tammiku-Taul J (2007) Cesium cation affinities and basicities. Int J Mass Spectrom 267:7–23

Gastberger M, Steinhäusler F, Gerzabek MH, Lettner H, Hubmer A (2000) Soil-to-plant transfer of fallout caesium and strontium in Austrian lowland and Alpine pastures. J Environ Radioact 49:217–233

Graly JA, Bierman PR, Reusser LJ, Pavich MJ (2010) Meteoric ^{10}Be in soil profiles—a global meta-analysis. Geochim Cosmochim Acta 74:6814–6829

Granger DE, Clifford SR, Kirchner JW, Finkel RC (2001) Modulation of erosion on steep granitic slopes by boulder armouring, as revealed by cosmogenic ^{26}Al and ^{10}Be. Earth Planet Sci Lett 186:269–281

Gruber S (2012) Derivation and analysis of a high-resolution estimate of global permafrost zonation. Cryosphere 6:221–233

Gyssels G, Poesen J, Bochet E, Li Y (2005) Impact of plant roots on the resistance of soils to erosion by water: a review. Prog Phys Geogr 2: 189–217

Haas JN, Rischoz I, Tinner W, Wick L (1998) Synchronous Holocene climatic oscillations recorded on the Swiss Plateau and at the timberline in the Alps. The Holocene 8:301–309

Haeberli W, Frauenfelder R, Kääb A, Wagner S (2004) Characteristics and potential climatic significance of "miniature ice caps" (crest- and cornice-type low-altitude ice archives). J Glaciol 50:129–136

Haeberli W, Egli M, Keller F, Krüsi B, Rothenbuehler C, Meilwes J, Gruber S (2007) Raum-zeitliche Informationen über schnelle Klimaänderungen in hochalpinen Umweltsystemen als strategisches Werkzeug für Analyse, Kommunikation, partizipative Planung und Managment im Tourismusgebiet Oberengadin. Schlussbericht GISALP, NFP48 (Nationales Forschungsprogramm "Alpen"). vdf-Verlag, Zürich

Haeberli W, Noetzli J, Arenson L, Delaloye R, Gaertner-Roer I, Gruber S, Isakesen K, Kneisel C, Krautblatter M, Phillips M (2010) Mountain permafrost: development and challenges of a young research field. J Glaciol 56:1043–1058

Hitz C, Egli M, Fitze P (2002) Determination of the sampling volume for representative analysis of alpine soils. Z Pflanz Bodenkund 165: 326–331

Hoelzle M, Haeberli W, Dischl M, Peschke W (2003) Secular glacier mass balances derived from cumulative glacier length changes. Global Planet Chang 36:295–306

Hoo WT, Fifield LK, Tims SG, Fujioka T, Mueller N (2011) Using fallout plutonium as a probe for erosion assessment. J Environ Radioact 102:937–942

Horiuchi K, Minoura K, Kobayashi K, Nakamura T, Hatori S, Matsuzaki H, Kawai T (1999) Last-glacial to post-glacial 10Be fluctuations in a sediment core from the Academician Ridge, Lake Baikal. Geophys Res Lett 26:1047–1050

IUSS Working Group WRB (2007) World reference base for soil resources 2006. First update 2007. World Soil Resources Reports No. 103. FAO, Rome, 116 pp

Jóhannesson T, Raymond C, Waddington E (1989) Time-scale for adjustment of glaciers to changes in mass balance. J Glaciol 35:355–369

Kääb A, Chiarle M, Raup B, Schneider C (2007) Climate change impacts on mountain glaciers and permafrost. Global Planet Chang 56:vii–ix

Kelley JM, Bond LA, Beasley TM (1999) Global distribution of Pu isotopes and 237Np. Sci Total Environ 237–238:483–500

Ketterer ME, Szechenyi SC (2008) Determination of plutonium and other transuranic elements by inductively coupled plasma mass spectrometry: a historical perspective and new frontiers in the environmental sciences. Spectrochim Acta B 63:719–737

Ketterer ME, Zhang J, Yamada M (2011) Application of transuranics as tracers and chronometers in the environment. In: Baskaran M (ed) Handbook of environmental isotope geochemistry, advances in isotope geochemistry. Springer, Berlin, pp 395–417

Kirchner G, Strebl F, Bossew P, Ehlken S, Gerzabek MH (2009) Vertical migration of radionuclides in undisturbed grassland soils. J Environ Radioact 100:716–720

Kneisel C (2010) The nature and dynamics of frozen ground in alpine and subarctic periglacial environments. The Holocene 20:423–445

Kneisel C, Hauck C, Vonder Mühll D (2000) Permafrost below the timberline confirmed and characterized by geoelectrical resistivity measurements, Bever Valley, eastern Swiss Alps. Permafr Periglac 11:295–304

Kohn JM (2010) Carbon isotope compositions of terrestrial C_3 plants as indicators of (paleo)ecology and (paleo)climate. Proc Natl Acad Sci U S A 107:19691–19695

Konz N, Schaub M, Prasuhn V, Baenninger D, Alewell C (2009) Caesium-137 based erosion-rate determination of a steep mountainous region. J Plant Nutr Soil Sci 172:615–622

Konz N, Baenninger D, Konz M, Nearing M, Alewell C (2010) Process identification of soil erosion in steep mountain regions. Hydrol Earth Syst Sci 14:675–686

Kubik PW, Christl C (2009) ^{10}Be and ^{26}Al measurements at the Zurich 6 MV Tandem AMS facility. Nucl Instrum Meth 268:880–883

Lal D (2001) New nuclear methods for studies of soil dynamics utilizing cosmic ray produced for radionuclides. In: Stott DE, Mohtar RH, Steinhardt GC (ed) Sustaining the global farm. 10th International Soil Conservation Organization Meeting, Purdue University and USDA-ARS National Soil Erosion Research Laboratory, pp 1044–1052

Lal R, Tims SG, Fifield LK, Wasson RJ, Howe D (2013) Applicability of ^{239}Pu as a tracer for soil erosion in the wet-dry tropic of northern Australia. Nucl Instrum Meth B 294:577–583

Lana-Renault N, Alvera B, Garcìa-Ruiz JM (2011) Runoff and sediment transport during the snowmelt period in a Mediterranean high-mountain catchment. Arct Antarct Alp Res 43:213–222

Lettner H, Bossew P, Hubmer AK (2000) Spatial variability of fallout caesium-137 in Austrian alpine regions. J Environ Radioact 47:71–82

Mabit L, Meusburger K, Fulajtar E, Alewell C (2013) The usefulness of ^{137}Cs as a tracer for soil erosion assessment: a critical reply to Parsons and Foster (2011). Earth Sci Rev 127:300–307

Maejima Y, Matsuzaki H, Higashi T (2005) Application of cosmogenic ^{10}Be to dating soils on the raised coral reef terraces of Kikai Island, southwest Japan. Geoderma 126:389–399

Maisch M (2001) The longterm signal of climate change in the Swiss Alps—glacier retreat since the end of the Little Ice Age and future ice decay scenarios. Geogr Fis Din Quat 23:139–151

McKean JA, Dietrich WE, Finkel RC, Southon JR, Caffee MW (1993) Quantification of soil production and down slope creep rates from cosmogenic ^{10}Be accumulations on a hillslope profile. Geology 21: 343–346

Meusburger K, Mabit L, Park JH, Sandor T, Alewell C (2013) Combined use of stable isotopes and fallout radionuclides as soil erosion indicators in a forested mountain site, South Korea. Biogeosciences 10:5627–5638

Monaghan MC, Krishnaswami S, Turekian KK (1985/1986) The global average production of ^{10}Be. Earth Planet Sci Lett 76:279–287

Nakanishi T, Matsubga T, Koarashi J, Atarashi-Andon M (2014) ^{137}Cs vertical migration in a deciduous forest soil following the Fukushima Dai-ichi Nuclear Power Plant accident. J Environ Radioact 128:9–14

Nishiizumi K, Imamura M, Caffee MW, Southon JR, Finkel RC, McAninch J (2007) Absolute calibration of ^{10}Be AMS standards. Nucl Instrum Meth B 258:403–413

Nötzli J, Gruber S (2005) Alpiner Permafrost – Ein Überblick. Jahrbuch des Vereins zum Schutz der Bergwelt 70:111–121

Ould-Dada Z (2002) Dry deposition profile of small particles within a model spruce canopy. Sci Total Environ 286:83–96

Pavich MJ, Brown L, Harden J, Klein J, Middleton R (1986) ^{10}Be distribution in soils from Merced River terraces, California. Geochim Cosmochim Acta 50:1727–1735

Ping CL, Michaelson GJ, Kimble JM, Romanovsky VE, Shur YL, Swanson DK, Walker DA (2008) Cryogenesis and soil formation along a bioclimate gradient in Arctic North America. J Geophys Res-Biogeo 113, G03S12

Ritchie JC, Ritchie CA (2007) Bibliography of publications of ^{137}Cesium studies related to erosion and sediment deposition. USDA-ARS Hydrology and Remote Sensing Laboratory, United States Department of Agriculture, Agricultural Research Service

Rogowski AS, Tamura T (1970) Environmental mobility of cesium-137. Radiat Bot 10:35–45

Schaller M, von Blanckenburg F, Hovius N, Kubik PW (2001) Large-scale erosion rates from in situ-produced cosmogenic nuclides in European river sediments. Earth Planet Sci Lett 188:441–458

Schaub M, Alewell C (2009) Stable carbon isotopes as an indicator for soil degradation in an alpine environment (Urseren Valley, Switzerland). Rapid Commun Mass Spectrom 23:1499–1507

Scheurer K, Alewell C, Bänninger D, Burkhardt-Holm P (2009) Climate and land-use changes affecting river sediment and brown trout in alpine countries—a review. Environ Sci Pollut Res 16:232–242

Schimmack W, Auerswald K, Bunzl K (2001) Can $^{239+240}$Pu replace ^{137}Cs as an erosion tracer in agricultural landscapes contaminated with Chernobyl fallout? J Environ Radioact 53:41–57

Schwarb M, Daly C, Frei C, Schär C (2000) Mittlere jährliche Niederschlagshöhe im europäischen Alpenraum 1971–1990. In Hydrologischer Atlas der Schweiz: Blatt 2.6

Shakhashiro A, Mabit L (2009) Results of an IAEA intercomparison exercise to assess Cs-137 and total Pb-210 analytical performance in soil. Appl Radiat Isot 67:139–146

Soil Survey Staff (2010) Keys to Soil Taxonomy, 11th edition. USDA (United States Department of Agriculture), NRCS (National Resources Conservation Service), Washington

Staunton S, Dumat C, Zsolnay A (2002) Possible role of organic matter in radiocaesium adsorption in soils. J Environ Radioact 58:163–173

Suter J (1981) Gletschergeschichte des Oberengadins: Untersuchungen von Gletscherschwankungen in der Err-Julier-Gruppe. Dissertation, University of Zürich, Physische Geographie, vol. 2

Tape KD, Verbyla D, Welker JM (2011) Twentieth century erosion in Arctic Alaska foothills: the influence of shrubs, runoff, and permafrost. J Geophys Res 116, G04024

Tims SG, Everett SE, Fifield LK, Hancock GJ, Bartley R (2010) Plutonium as a tracer of soil and sediment movement in the Herbert River, Australia. Nucl Instrum Meth B 268:1150–1154

Tsai H, Maejima Y, Hseu ZY (2008) Meteoric ^{10}Be dating of highly weathered soils from fluvial terraces in Taiwan. Quat Int 188:185–196

Turner M, Rudin M, Cizdziel J, Hodge V (2003) Excess plutonium in soil near the Nevada Test Site, USA. Environ Pollut 125:193–203

Voigt G, Fesenko S (eds) (2009) Remediation of contaminated environments. Radioact Environ 14:477

Walling DE, He Q (1999) Improved models for estimating soil erosion rates from cesium-137 measurements. J Environ Qual 28:611–622

Walling DE, He Q (2000) The global distribution of bomb-derived 137Cs reference inventories. Final Rep. IAEA Technical Contract 10361/RO-R1

Walling DE, Quine TA (1990) Calibration of caesium-137 measurements to provide quantitative erosion rate data. Land Degrad Rehabil 2:161–175

Wischmeier WH, Smith DD (1978) Predicting rainfall erosion losses: a guide to conservation planning. Agriculture Handbook No. 537. USDA/Science and Education Administration, US. Govt. Printing Office, Washington, DC, 58

Yoshihara T, Matsumura H, Hashida S, Nagaoka T (2013) Radiocesium contaminations of 20 wood species and the corresponding gamma-ray dose rates around the canopies at 5 months after the Fukushima nuclear power plant accident. J Environ Radioact 115:60–68

Zapata F (2002) Handbook for the assessment of soil erosion and sedimentation using environmental radionuclides. Kluwer, Dordrecht

Zhang X, Higgitt DL, Walling DE (1990) A preliminary assessment of the potential for using caesium-137 to estimate rates of soil erosion in the Loess Plateau of China. Hydrol Sci J 35:243–252

Zhiyanski M, Bech J, Sokolovska M, Lucot E, Bech J, Badot P-M (2008) Cs-137 distribution in forest floor and surface soil layers from two mountainous regions in Bulgaria. J Geochem Explor 96:256–266

Ziegler AD, Giambelluca TW (1998) Influence of revegetation efforts on hydrologic response and erosion, Kaho'Olawe Island, Hawaii. Land Degrad Dev 9:189–206